Monitoring root rot in flat-leaf parsley via machine vision by unsupervised multivariate analysis of morphometric and spectral parameters

Avinash Agarwal
avinash.agarwal.1612@gmail.com
Newcastle University Faculty of Science Agriculture and Engineering https://orcid.org/0000-0002-9855-0144
Filipe de Jesus Colwell
InFarm - Indoor Urban Farming B.V.
Julian Bello Rogdriguez
Newcastle University
Sarah Sommer
Newcastle University
Viviana Andrea Correa Galvis
InFarm - Indoor Urban Farming B.V.
Tom Hill
Newcastle University
Neil Boonham
Newcastle University
Ankush Prashar
Newcastle University

Research Article

Keywords: root rot, machine vision, disease detection, hydroponics, vertical farming, multivariate analysis

Posted Date: October 19th, 2023

DOI: https://doi.org/10.21203/rs.3.rs-3445489/v1

Version of Record: A version of this preprint was published at European Journal of Plant Pathology on February 19th, 2024. See the published version at https://doi.org/10.1007/s10658-024-02834-z.

Abstract

Use of vertical farms is increasing rapidly as it enables year-round crop production, made possible by fully controlled growing environments situated within supply chains. However, intensive planting and high relative humidity make such systems ideal for the proliferation of fungal pathogens. Thus, despite the use of bio-fungicides and enhanced biosecurity measures, contamination of crops does happen, leading to extensive crop loss, necessitating the use of high-throughput monitoring for early detection of infected plants. In the present study, progression of foliar symptoms caused by *Pythium irregulare*-induced root rot was monitored for flat-leaf parsley grown in an experimental hydroponic vertical farming setup. Structural and spectral changes in plant canopy were recorded non-invasively at regular intervals using a 3D multispectral scanner. Five morphometric and nine spectral features were selected, and different combinations of these features were subjected to multivariate data analysis via principal component analysis to identify temporal trends for early disease detection. Combining morphometric and spectral features enabled a clear segregation of healthy and diseased plants at 4–7 days post inoculation (DPI), whereas use of only morphometric or spectral features allowed this at 7–9 DPI. Minimal datasets combining the six most effective features also resulted in effective grouping of healthy and diseased plants at 4–7 DPI. This suggests that selectively combining morphometric and spectral features can enable accurate early identification of infected plants, thus creating the scope for improving high-throughput crop monitoring in vertical farms.

INTRODUCTION

Vertical farming facilitates year-round crop production, with higher yields per unit area and more efficient utilisation of resources such as land, water, and nutrients than conventional farming (Specht et al., 2014; Rajan et al., 2019). Such systems employ artificial lighting and soilless culture techniques to maximize crop production under controlled environmental conditions (van Delden et al., 2021). Since vertical farms do not require large expanses of land, production points can be located closer to consumers on brown-field sites, potentially reducing the carbon footprint resulting from food transport (van Delden et al., 2021). Further, physical isolation from the external environment provides a high level of biosecurity, reducing the risk of plant pests, diseases, and pathogens associated with human food-borne illness compared to open field production systems.

Despite the presence of physical barriers, achieving complete exclusion of pathogens from vertical farms is practically challenging. Consequently, crop losses from unintentional bacterial or fungal contamination may occur due to inefficient phytosanitary measures, inadequately treated seeds and substrates, or air-borne spores introduced through the ventilation system (Roberts et al., 2020). In addition, the combination of high-density production environment with recirculation of nutrient solutions within vertical farms exacerbates the situation by facilitating rapid pathogen spread. Furthermore, high humidity and favourable ambient temperature supports pathogen proliferation in such systems (Paulitz, 1997; Roberts et al., 2020). Thus, there is a high risk of extensive crop loss when biosecurity measures are breached in vertical farms. Hence, early detection of diseased plants is crucial for controlling pathogen spread and minimising the risk of crop loss in vertical farms.

Conventionally, identification and scoring of plant diseases is performed by experts via visual inspection of samples (Bock et al., 2010). However, this approach is reliant on the presence of visual symptoms, which can be subjective, inconsistent across practitioners, and inadequate for detecting diseases during their latent period when the pathogens are spreading without causing visible symptoms. Further, the process is time-consuming and labour-intensive, and is thus, practically feasible only for small sample sizes. In addition, large-scale hydroponic farms often maintain strict restrictions on the access of personnel around growing benches to ensure biosafety, making visual scoring highly improbable. As an advancement to manual inspection, molecular methods have revolutionized plant disease diagnosis, accelerating pathogen detection and facilitating the screening of asymptomatic plants, making the process less subjective (Martinelli et al., 2015). However, such techniques require specialised infrastructure and experienced laboratory personnel, and are expensive to perform routinely, making it difficult for widespread use in commercial cultivation. In addition, the process would be destructive, and would be implementable on just a few samples in every batch of plants. Hence, the necessity of an alternative easy-to-use/automatable technology for crop monitoring has driven the development of machine vision-based techniques for identifying characteristic stress symptoms in plants to allow real-time assessment of diseases and health status. These methods can be deployed to collect data in real-time without generating significant additional costs.

Plant diseases typically induce various visible morphological changes, such as stunted growth and reduced canopy cover, as well as spectral aberrations associated with disease symptoms, such as generalised or localised (lesions), tissue chlorosis, and necrosis (Mutka and Bart, 2015). Plant image analysis for disease detection focuses on finding these irregularities in growth patterns and spectral properties. In this context, multispectral imaging has emerged as a low-cost, high-throughput alternative for assessing plant health by identifying abnormalities in leaf colour features (Martinelli et al., 2015; Agarwal et al., 2021; Waiphara et al., 2022). Recent studies have also attempted to highlight the efficacy of 3D imaging for monitoring structural changes in plants under stress (Su et al., 2019; Husin et al., 2020). In addition, application of advanced data processing techniques such as multivariate data analysis (MDA) and machine learning (ML) for plant image analysis has played a crucial role making in-depth assessment of image features feasible (Singh et al., 2021). Suitability of such plant image analysis approaches for non-destructive monitoring of plant responses to biotic stressors has been investigated in detail for crops grown in field conditions (Mutka and Bart, 2015; Zhang et al., 2019; Singh et al., 2021). However, reports for hydroponic vertical farming systems are very limited.

Prevalence of root diseases is a major concern for commercial hydroponic operations (Suárez-Cáceres et al., 2021). Zoosporic and wilt pathogen species such as *Pythium*, *Phytophthora*, and *Fusarium* have been most frequently reported to cause vascular and root diseases in various crops grown hydroponically (Paulitz, 1997; Suárez-Cáceres et al., 2021). In particular, root rot and damping-off due to various *Pythium spp.* is a serious issue affecting hydroponic production of various Apiacae crops, including flat-leaf parsley (*Petroselinum crispum* var. *neapolitanum*), a popular culinary herb (Minchinton et al., 2013). Early detection of root diseases is more challenging compared to foliar diseases as it is difficult to actively monitor roots, where the symptoms initially occur. However, morphological and spectral changes that appear on the canopy could be used as indirect indicators of root infections, and be monitored for detecting such diseases (Salgadoe et al., 2018).

In this study, we examined changes in morphometric and spectral attributes of flat-leaf parsley upon infection with *Pythium irregulare* in an experimental hydroponic vertical farming system. We aimed to ascertain the post-infection window for reliable early identification of diseased plants using concurrent 3D and multispectral imaging. The scope of detecting infected plants by using morphometric and spectral attributes independently and simultaneously was explored via multivariate data analysis using principal component analysis (PCA), along with step-wise variable reduction to determine efficacy of minimal datasets for reliable disease detection at early stages of infection.

MATERIAL AND METHODS

Plant growth trials

Flat-leaf parsley seedlings were raised from seeds in coco-peat plugs (Van der Knapp, The Netherlands) following dark germination under sterile conditions in a nursery chamber (Aralab-InFarm UK Ltd., London, UK). A seedling density of ~ 25 seedlings/plug was maintained to replicate commercial production standards. After reaching a height of *ca.* 2 cm, the seedlings were transferred to a customised experimental vertical farming setup (Fig. 1) having "deep water culture" hydroponic units in a growth chamber with regulated environment (Newcastle University, Newcastle upon Tyne, UK). Each hydroponic unit comprised of a polypropylene container (dark grey, opaque; inner dimensions: L×W×H 56×36×11 cm) with a tray-lid (white, opaque) having a 7×4 array of circular empty slots. The container was filled with 18 L commercial hydroponics solution. Each unit received 26 seedling plugs, and a submersible water pump was used for root aeration along with a circulating water bath for maintaining constant water temperature. Plants were grown for 20 days at a temperature of 22 ± 1°C and 75 ± 5% relative humidity, under 300–350 µmol.m^{-2}s^{-1} broad spectrum LED lighting (L28–NS12, Valoya Ltd., Finland) following a 16/8 hrs day-night cycle. Two experimental trials were carried out as follows: 1) preliminary trial (PT) to identify effects of infection on the morphometric and spectral attributes over time; 2) main trial (MT) to select the features and perform multivariate data analysis for plant health assessment and disease detection. In each trial, two units received *P. irregulare* inoculum (described later), and two were used as control.

Pathogen isolation and inoculation

P. irregulare was isolated from diseased plants growing in a commercial hydroponic vertical farm, and were cultured on PARP + B (corn meal agar with pimaricin, 5 mg/L; ampicillin, 250 mg/L; rifampicin, 10 mg/L; pentachloronitrobenzene, 50 mg/L; and benomyl 10 mg/L) semi-selective medium (Matthiesen et al., 2016). Identity of the isolate was confirmed following PCR-based amplification of specific ITS and COX II genes (Online resource 1: Table S1) as reported earlier (White et al., 1990; Martin, 2000). The pathogen was grown in bulk using clarified-V8 broth, with minor modifications to the protocol described by McGehee et al. (2019). Briefly, a 4-mm plug of the PARP + B medium inoculated with the pathogen was transferred to a sterile Petri dish. Subsequently, the Petri dish was filled with 20 mL of V8 broth, and incubated in the dark for 5 days at 25°C. Subsequently, the mycelial mats were liquified in ddH_2O for 2 min to obtain a final concentration of ~ 1 × 10^4 mycelial fragments/mL. The resulting slurry was used to inoculate the seedling plugs at 1 mL/plug at 5 days post nursery for the preliminary trial, and at 4 days post nursery in the main trial to induce the symptoms of infection earlier. Further, in the main trial two samples were randomly selected from each inoculated tray at 8 days post inoculation (DPI) to confirm the presence of pathogen using the same PCR-based method.

Multispectral 3D scanning

Each hydroponic unit was scanned using a PlantEye F500 multispectral LiDAR scanner (Phenospex, The Netherlands, www.phenospex.com) to record the spectral reflectance and 3D features of the plant canopy at 8, 11, and 15 DPI in the PT, and at 2, 4, 7, 9, and 11 DPI in the MT. Plants were scanned maintaining a fixed distance of 100 cm between the scanner and the plant base, and the scanner moved at a speed of 50 mm/s (Y-axis). This provided an approximate resolution of 0.7 mm X-axis, 1 mm Y-axis, and 0.2 mm Z-axis. Spectral reflectance was measured in the blue (B; λ = 460–485 nm), green (G; λ = 530–540 nm), red (R; λ = 620–645 nm), and near-infrared (NIR; λ = 720–750 nm) wavebands. Morphometric information was recorded using a laser scanner (λ = 940 nm) to create a 3D point-cloud. The scanner had an in-built LED light sources for all corresponding wavebands. The scans were processed in the HortControl software (Phenospex), and triangulation of point-cloud data yielded 3D plant models. Each scan was divided into a 7×4 array of identical sectors corresponding to each plant for obtaining sample-wise morphometric and spectral data.

Morphometric and spectral feature extraction

The HortControl software was used to obtain nine morphometric parameters: mean plant height, maximum plant height, total leaf area (TLA), leaf area index (LAI), projected leaf area (PLA), digital biomass (DB), leaf angle, leaf inclination (LInc), and light penetration depth (LPD) (Table 1). Additionally, spectral measurements were processed by the software to obtain five spectral indices as follows: Green Leaf Index (GLI, [(2×G)-R-B]/[(2×G) + R + B]), Hue, Normalised Difference Vegetation Index (NDVI, [NIR-R]/[NIR + R]), Normalized Pigment Chlorophyll ratio Index (NPCI, [R-B]/[R + B]), and Plant Senescence Reflectance Index (PSRI, [R-G]/NIR) (https://phenospex.helpdocs.com/planteye). Spectral information was augmented by extracting the raw R, G, B, and NIR reflectance data from the point-cloud files (.ply) using Python programming (www.python.org) and by calculating R/G, G/R, R + G + B, R + G-B, R + G, G minus R (GMR) (Agarwal and Dutta Gupta, 2018), and augmented green-red index (AGRI, [G-R]×G/R).

Table 1
Definitions of morphometric indices measured by the scanner

Parameter	Definition
Mean plant height	Average height of the top 10% points within the canopy
Maximum plant height	Height at the absolute highest point within the canopy
Total leaf area (TLA)	Sum of all triangulated surfaces on the canopy
Leaf area index (LAI)	TLA/sector area
Projected leaf area (PLA)	Two-dimensional projection of TLA
Digital biomass (DB)	Mean plant height × TLA
Leaf angle	Weighted average of all angles for every face in the triangulated plant mesh
Leaf inclination (LInc)	TLA/PLA
Light penetration depth (LPD)	Lowest point in the canopy detectable by the laser

PCA for disease detection

As a preliminary step for reducing the number of PCA features, all twenty-five morphometric and spectral attributes were subjected to correlation analysis using the Data Analysis ToolPak (Microsoft Excel 365, Microsoft Corp., USA) to identify attributes exhibiting identical linear trends. Attributes with strong linear relations ($r < -0.95$, $r > 0.95$) were selectively omitted to minimise redundancy. The attributes that were retained, henceforth referred to as "selected features", were subjected to PCA to ascertain the possibility of distinguishing between healthy and infected plants at different intervals post infection. PCA was performed in Python using the Scikit-learn module (Pedregosa et al., 2011), at a threshold of > 99% variance explained. The following subsets of selected features were used for PCA at each imaging interval: 1) all morphometric attributes (M_all); 2) all spectral attributes (S_all); 3) all the selected features (MS_all). Eigen values and percentage of variance explained were recorded for each principal component (PC), along with the PC loadings of each feature. PCA loadings obtained from the MS_all dataset were used to calculate the weighted loading (WL) for each feature at every interval as follows:

$$\mathrm{WL} = \sqrt{\sum_{i=1}^{n} (Ex_i \times L_i)^2} \quad \text{...(Eq. 1)}$$

Here, Ex_i and L_i indicate proportion of variance explained (0–1) and loading of the feature for the i^{th} PC, respectively, and n indicates the total number of PCs obtained. Features were assigned ranks based on WL values to indicate their performance at each interval; higher WL earned a better rank, and vice versa. Overall performance ranks were assigned as per the mean of ranks obtained across all intervals. Based on this, PCA was performed using the best ranked variables collated in two subsets containing < 25% of the actual features (henceforth referred to as "minimal datasets") as follows: 1) three best morphometric and three best spectral attributes (MS_3–3); and 2) top six attributes (MS_top6). This was done to assess the impact of total number of features and the balance between morphometric and spectral features on the analysis

Biplots indicating the loadings and scores for the first two PCs were plotted for each PCA along with the 95% confidence ellipse for each class, i.e., healthy and infected, for all five feature subsets at each imaging interval to visualise the temporal trends in unsupervised (without prior labelling) segregation of the two classes.

RESULTS

Morphometric and spectral attributes

Plant growth and appearance was markedly affected by *P. irregulare* infection 7 DPI onwards, as observed in both trials (Fig. 2; Online resource 1: Fig. S1). Clear signs of stress and tissue damage were visible in leaves as well as roots (Online resource 1: Fig. S2). Morphometric attributes such as DB, mean plant height, and LAI indicated that growth was stunted in the infected plants, with the difference compared to control becoming more prominent in height and DB with the progression of infection (Fig. 2a–c). Spectral attributes such as Hue, GLI, NDVI, and AGRI remained higher in healthy plants relative to the infected samples (Fig. 2f–h, n), whereas the opposite trend was observed for PSRI, G, and NIR, i.e., the values for the healthy samples were generally lower than the infected plants (Fig. 2i, k, l). Other features, viz., LInc, LPD, NPCI, and GMR exhibited high degree of overlap between the control and infected samples at most intervals (Fig. 2d, e, j, m).

Feature selection for PCA

As per the results of linear correlation analysis (Online resource 1: Table S2), five morphometric and nine spectral features, viz., DB, mean plant height, LAI, LInc, LPD, GLI, Hue, NDVI, NPCI, PSRI, G, NIR, GMR and AGRI, were selected for PCA. Eleven features, i.e., maximum plant height, leaf angle, TLA, PLA, R, B, R/G, G/R, R + G + B, R + G-B, and R + G, were omitted from subsequent analyses based on their strong correlation ($r < -0.95$, $r > 0.95$) with at least one of the selected features (Online resource 1: Table S3).

Early disease detection using all selected features

PCA biplots for analyses using morphometric features (M_all), spectral features (S_all), and both datasets combined (MS_all) revealed the scope of accurately segregating healthy and infected plants by machine vision at later stages of infection, i.e., 7 DPI and higher (Fig. 3; Online resource 1: Fig. S3). Analysing the

MS_all dataset enabled better differentiation between the healthy and diseased samples than the M_all and S_all datasets at 7 DPI, as indicated by the 95% confidence ellipse. All biplots for subsequent intervals showed this trend, suggesting that M_all and S_all could also be used to reliably identify infected plants at 9 and 11 DPI, i.e., when the effects of infection became more prominent. Cumulative variance explained (CVE) by PC1 and PC2 for the M_all dataset did not exhibit a clear trend, and varied between 76–83% for the five intervals (Online resource 1: Table S4). In contrast, CVE values increased over 2 to 11 DPI for S_all and MS_all datasets, i.e., from 77.09–94.54% and from 64.71–81.6%, respectively (Online resource 1: Tables S5 and S6), suggesting clearer sample trends with disease progression.

Early disease detection using minimal datasets

WL values calculated based on the PCA with MS_all dataset revealed a clear variation in the performance of all the selected features at different stages of infection (Table 2). The magnitudes of WL were close to 0.11 and 0.15 at 2 DPI for the lowest and highest ranked features, respectively, indicating relatively small variability in performance amongst the features. The range gradually increased with the duration of infection, and WL values reached 0.08 and 0.22 at 11 DPI for the weakest and best features, respectively, suggesting a clear improvement in the performance of some features. Rankings based on WL values (Table 2) indicated that features such as GLI and NDVI performed well consistently (rank < 5), whereas LPD and LInc had consistently poor performance (rank > 11); the performance of all other features varied markedly at each interval.

Considering the overall performance and ranking, three morphometric features, viz., DB, mean plant height, and LAI, and four spectral features, viz., GLI, NDVI, AGRI, and G, were selected for further analyses using minimal datasets as follows: the MS_3–3 dataset consisted of DB, mean plant height, LAI, GLI, NDVI, and AGRI, whereas the MS_top6 dataset had G instead of LAI. PCA using the minimal datasets yielded effective segregation (95% confidence interval) of the healthy and infected samples at 7 DPI (Fig. 4). Notably, the MS_3–3 dataset resulted in a more compact clustering of the two sample classes compared to the MS_top6 at 9 and 11 DPI (Online resource 1: Fig. S4). CVE by PC1 and PC2 increased from 83.82–95.29% for MS_3–3 over 2 to 11 DPI (Online resource 1: Table S7), whereas the values increased from 78.67–95.11% for the MS_top6 dataset over the same interval (Online resource 1: Table S8), indicating steady improvement in sample clustering with disease progression.

Table 2
Weighted loadings (WL) and ranks of features based on PCA with MS_all dataset.

DPI		DB	Ht	LAI	LInc	LPD	GLI	Hue	NDVI	NPCI	PSRI	G	NIR	GMR	AGRI
2	*WL*	0.1447	0.1204	0.1418	0.1155	0.1068	0.1497	0.125	0.1435	0.1309	0.1188	0.1362	0.1122	0.143	0.147
	Rank	3	10	6	12	14	1	9	4	8	11	7	13	5	2
4	*WL*	0.162	0.1352	0.1591	0.0799	0.0958	0.167	0.1458	0.1728	0.1068	0.1595	0.1663	0.1219	0.1171	0.144
	Rank	4	9	6	14	13	2	7	1	12	5	3	10	11	8
7	*WL*	0.1849	0.1891	0.1698	0.0776	0.0852	0.1993	0.1771	0.1981	0.1343	0.1817	0.1931	0.1662	0.1014	0.180
	Rank	5	4	9	14	13	1	8	2	11	6	3	10	12	7
9	*WL*	0.2063	0.2111	0.1837	0.0799	0.1395	0.2203	0.2053	0.2169	0.1459	0.2023	0.2086	0.1949	0.1734	0.212
	Rank	6	4	10	14	13	1	7	2	12	8	5	9	11	3
11	*WL*	0.2017	0.2112	0.1683	0.0805	0.1514	0.2216	0.2086	0.2193	0.1414	0.207	0.2043	0.2024	0.197	0.215
	Rank	9	4	11	14	12	1	5	2	13	6	7	8	10	3
Average rank		5.4	6.2	8.4	13.6	13	1.2	7.2	2.2	11.2	7.2	5	10	9.8	4.6
Overall rank		5	6	9	14	13	1	7	2	12	8	4	11	10	3

DPI, days post inoculation; Attributes (ordered as per the table) - DB: Digital biomass; Ht: Mean plant height; LAI: Leaf area index; LInc: Leaf inclination; LPD: Light penetration depth; GLI: Green leaf index; NDVI: Normalised difference vegetation index; NPCI: Normalized pigment chlorophyll ratio index; PSRI: Plant senescence reflectance index; G: Green; NIR: Near infrared; GMR: G minus R; AGRI: Augmented green-red index.

DISCUSSION

The application of machine vision for real-time high-throughput non-invasive monitoring of plant health status and growth has been explored for a wide variety of crops (Bock et al., 2010; Zhang et al., 2019; Singh et al., 2021; Waiphara et al., 2022). In this context, 3D scanners have been implemented for characterising growth and stress-related structural changes in a variety of crops, including maize (Friedli et al., 2016; Su et al., 2019), wheat, soybean (Friedli et al., 2016), peanut (Yuan et al., 2019), oil palm (Husin et al., 2020), sugar beet (Xiao et al., 2020), and potato (Mulugeta Aneley et al., 2022). However, the use of 3D imaging for crop disease detection is still in the conceptualisation stage (Zhang et al., 2019). In contrast, use of multispectral sensors has been investigated in depth for detecting various crop diseases, including sheath blight (Qin and Zhang, 2005), powdery mildew, leaf rust (Franke and Menz, 2007), root rot (Yang et al., 2010), late blight (Sugiura et al., 2016), mosaic virus disease (Raji et al., 2016), huanglongbing (DadrasJavan et al., 2019), and light leaf spot (Veys et al., 2019). Further, only a small percentage of such studies have attempted to amalgamate the information obtained via simultaneous implementation of both types of sensors (Lazarević et al., 2021; Manavalan et al., 2021).

Herein, we aim to highlight the potential of machine-vision for co-monitoring morphometric and spectral attributes using *P. irregulare* infection in flat-parsley as a model system to assess the health of crops grown hydroponically in a vertical farm, with emphasis on early detection of disease symptoms using MDA following temporal data acquisition. In the current study, various exploratory experiments were conducted using different inoculation methods, inoculum concentrations, and inoculation intervals, and were tested to establish the pathogenesis model to be used for the intended analysis. The design yielding the best result (described in the methods section) was considered as the preliminary trial, and was replicated in the main trial for temporal MDA. The preliminary trial presented clear indications of shoot and root tissue damage in infected plant samples, and provided a tentative timeframe for attempting early disease detection (Online resource 1: Fig. S1). In this trial, data was collected from 8 DPI onwards when disease symptoms such as leaf yellowing and slower growth compared to the control became very clear upon visual inspection.

In the main trial, recording morphometric and spectral data intermittently from 2 DPI onwards helped provide a clear picture of how the infection affected the plants over time (Fig. 2). While some parameters such as DB and plant height increased steadily in healthy samples from 2 to 11 DPI, attributes such as LAI, GLI, NDVI, and PSRI plateaued around 4 to 7 DPI. In contrast, the infected samples did not exhibit any considerable change in DB and plant height, whereas a steady decline in GLI and AGRI was recorded after 4 DPI. As recorded in the healthy plants, LAI, NDVI, and PSRI showed plateauing around 4 to 7 DPI in the infected plants as well, although the magnitudes differed considerably between the two groups. Such variations in relative temporal trends of the different imaging attributes highlight the complexity in automatic identification of diseased plants using individual parameters, because the efficacy of disease detection using each attribute varies with time. However, co-interpretation of these temporal trends following MDA helped overcome this limitation.

Selected features were subjected to PCA to obtain a holistic overview of the temporal trends via dimensional reduction. As an initial feature elimination step prior to PCA, eleven out of the twenty-five recorded attributes were omitted based on their strong correlation ($r < -0.95$, $r > 0.95$) with one or more selected features (Online resource 1: Tables S2 and S3). This helped minimise redundancy in information, reduced the computational load, and simplified data analysis. In addition, removing redundant variables also reduced the likelihood of biasing feature rankings without affecting the quality of analysis, which would otherwise have a negative impact on subsequent computations and interpretations. This was confirmed by performing PCA with all twenty-five features (data not shown), wherein extensive overlap between highly correlated features was observed, with no significant improvement in the clustering of healthy and infected samples.

Results of PCA using all data subsets, viz., M_all, S_all, MS_all (Fig. 3; Online resource 1: Fig. S3), MS_3–3, and MS_top6 (Fig. 4; Online resource 1: Fig. S4), revealed that the infected samples could be segregated from the control most reliably at later stages, i.e., 7 DPI onwards, when the symptoms became prominent. Since members of the *Pythium* genera are root necrotrophs, they preferentially attack the root tissue and cause root rot (Okubara and Paulitz, 2005). This leads to a gradual systematic decline in overall plant health and possibly even death. Considering the indirect impact of *Pythium* on above-ground plant parts, a delay in the appearance of foliar symptoms is highly likely. Hence, spectral attributes such as GLI, Hue, and AGRI (Fig. 2) present a decline in infected plants from around 4 DPI, which indicates deteriorating plant health. Although a steady increase in the morphometric attributes was noticeable for healthy plants 4 DPI onwards, these attributes did not change considerably in the infected plants (Fig. 2). Nevertheless, multivariate analysis enabled a sizeable proportion of the infected samples to be distinguished from the healthy samples even at 2 DPI, as depicted by the PCA biplots. This suggests that samples which got affected by the pathogen more severely could be identified using MDA as early as 2 DPI.

Distinguishing infected samples from healthy ones using the absolute values of individual attributes would have been particularly challenging at 2 DPI owing to the considerable overlap between the range of values between the two classes (Fig. 2). In contrast, multivariate data analysis via PCA allowed the variations for all selected features to be assessed simultaneously and be concatenated to provide an overall depiction of the difference between the samples (Fig. 3, 4). Dimensionality reduction by PCA further simplified data interpretation by generating PCs, i.e., hypothetical variables formed by linear combinations of all features, which allowed the information from numerous real variables (in this case five to fourteen) to be presented in a two-dimensional biplot. Thus, co-assessing morphometric and spectral attributes via PCA helped accentuate even minor differences between the healthy and diseased plant samples, which could potentially enable early identification of infected plants.

Abnormalities in plant health may not be clearly perceptible very early when only morphological traits are being used. In addition, a major conundrum related to this is that morphological features such as plant height, leaf area, and dry biomass tend to remain unchanged at early stages in stressed plants, which necessitates the presence of a healthy plant for reference. In contrast, alterations in leaf pigmentation, which closely represent changes in plant physiological status, start occurring following the onset of stress and lead to characteristic deviations in spectral properties (Nilsson, 1995). Thus, temporal monitoring of spectral attributes in conjunction with morphometric measurements could provide a better insight into plant health status. This is indicated by the PCA biplots for 4 and 7 DPI (Fig. 3), wherein MS_all and S_all datasets result in better clustering of the healthy and infected plants than M_all. It may also be noted that multispectral measurements allow numerous hypothetical spectral indices to be generated from only a few wavebands. For instance, in this study reflectance from four spectral regions, viz., R, G, B, and NIR, were used to calculate twelve theoretical spectral indices. In contrast, generation of hypothetical morphometric features may be more challenging due to the high likelihood of being physically unrealistic or inconceivable.

In the present study, the smaller number of morphometric features ($n = 5$) compared to spectral features ($n = 9$) used for MDA could have arguably biased the results in favour of spectral attributes. In addition, the MS_all dataset had a high proportion of spectral attributes, which could have skewed the outcome as well. Thus, in addition to testing the possibility of using a smaller number of features for detecting infected plants accurately, analyses with fewer features ($n = 6$), i.e., MS_3–3 and MS_top6, were performed to better understand how the total number of features and the balance between morphometric and spectral features impacted the analysis. Similar to the test with MS_all, PCA with both minimal datasets produced non-overlapping clusters (95% confidence interval) for the healthy and infected samples at 7 DPI, albeit using less than half the features as MS_all ($n = 14$). Since features having better overall WL in previous analyses (Table 2) were selected for this step, it may be inferred that the quality of features being used was more important than the total number of features.

Notably, features such as NPCI, LPD, and LInc, which were ranked the lowest based on WL (Table 2), exhibited irregular trends or had considerable overlap between the healthy and infected plants (Fig. 2). In contrast, the best-ranked features, viz., GLI, NDVI, AGRI, G, DB, and mean plant height (Table 2), showed distinct temporal trends and had limited overlap between the two classes (Fig. 2), which corroborates the selection of features based on WL. Further, the analysis was not affected significantly by the ratio of morphometric and spectral features (Fig. 4) as long as features exhibiting clear trends were being used. Notably, all three datasets combining both types of features (MS_all, MS_3–3, MS_top6) resulted in better segregation of healthy and infected samples, as indicated by the biplot for 7 DPI (Fig. 3, 4). This clearly indicates that using a combination of morphometric and spectral attributes improves the scope for early identification of unhealthy plants.

Various earlier studies have reported the use of plant image analysis via ML for disease detection (Singh et al., 2021; Ahmad et al., 2023). Application of advanced ML methods such as deep learning has greatly improved information processing for plant health assessment following data acquisition via machine vision (Yamamoto et al., 2017; Ghosal et al., 2018; Nagasubramanian et al., 2019). Although very advantageous for high-throughput plant stress detection, application of ML has various inherent limitations as well. For instance, supervised ML models essentially require the training samples to be manually annotated by an expert, making the method labour-intensive, subjective, and prone to errors (Singh et al., 2021). In addition, numerous studies have reported the successful application of ML-based disease detection using a very specific experimental setup, which would not be as effective for other diseases, plant species, or even a different stage of plant growth, thus limiting the versatility of the approach (Barbedo, 2013). Further, many of the algorithms implement “black-box” models that are difficult to depict, making their comprehension and implementation challenging for plant scientists with limited knowledge of ML (Singh et al., 2021).

In the present study, a simplified model-free approach employing MDA via PCA was adopted for identifying diseased plants that addresses issues mentioned previously. Salient advantages of the image analysis method adopted herein are as follows: 1) unsupervised data processing ensures fully objective analysis, with no human intervention and minimal preprocessing; 2) it is ready-to-use and does not require huge training datasets for model generation; 3) instead of generating a “black-box” model, it yields PCs that are linear combinations of the original features used; 4) requires limited computational expertise to understand and implement; 5) it is highly non-specific, i.e., the method can be implemented for other crops and diseases. Since this study focusses on disease detection for an indoor farming system with controlled lighting, data pre-processing was minimal, i.e., only linear correlation analysis was needed for reducing redundancy. Hence, the method could be implemented for high-throughput non-invasive detection of diseased plants with relative ease. However, if the protocol is adapted for operations with a variable light source (e.g., sunlight) as in the field or a glasshouse, colour balancing would be needed to compensate for variations in light environment between imaging intervals.

Although machine vision is very advantageous for crop monitoring, practical application of the technology in vertical farms poses certain challenges that are not encountered in field studies (Tian et al., 2022). For instance, installation of imaging sensors within the growing area is not feasible because such crop production systems aim at maximising vertical space utilisation and have crops growing in multiple tiers. Additionally, illumination spectrum could be another limiting factor for *in situ* imaging in vertical farms that employ non-white LED lighting, as leaf spectral reflectance characteristics would change according to incident light, necessitating reconfiguration of spectral indices that have been established using white light. A solution to these issues is the use of mobile cultivation beds that may be transferred intermittently to a fixed imaging platform for crop monitoring. Camera resolution and planting density would also affect the overall accuracy of the process, and image analysis protocols would require careful spatial calibration as per planting layout to identify trends at individual plant level. The present study highlights the efficacy of unsupervised and simultaneous implementation of spectral and morphometric features for early detection of root rot in hydroponics using flat-parsley as a model system. Investigations with other plant species, diseases, and imaging systems will be especially helpful in providing further insights into the scope of applying machine vision for early disease detection in vertical farms.

Declarations

Funding

This work was funded by Innovate UK (Technology Strategy Board – CR&D) [grant number: TS/V002880/1].

Acknowledgments

We thank the InFarm UK team for supplying seedlings and providing technical support along with InFarm Crop Science team for their support. We acknowledge all the partners (RoboScientific, Marks and Spencer, and InFarm) for their feedback and support in the project. We also thank the staff at Newcastle University for their technical, administrative, and logistical support.

Author contributions

NB, VACG, TH, and AP conceived the project. NB, AP, VACG, FdJC, and JBR designed the study. AA, FdJC, and JBR performed the experiments. JBR and SS performed pathogen strain identification. AA performed image and data analysis. AA drafted the manuscript with key inputs from SS on pathology work. All authors contributed to amendments and revisions. All authors approved the final submitted version.

Competing interests

The authors declare that there are no competing interests.

Data availability

The datasets generated during and/or analysed during the current study are available from the corresponding author upon reasonable request.

References

1. Agarwal, A., Dongre, P. K., & Dutta Gupta, S. (2021). Smartphone-assisted real-time estimation of chlorophyll and carotenoid concentrations and ratio using the inverse of red and green digital color features. *Theoretical and Experimental Plant Physiology*, *33*, 293–302. https://doi.org/10.1007/s40626-021-00210-4.
2. Agarwal, A., & Dutta Gupta, S. (2018). Assessment of spinach seedling health status and chlorophyll content by multivariate data analysis and multiple linear regression of leaf image features. *Computers and Electronics in Agriculture*, *152*, 281–289. https://doi.org/10.1016/j.compag.2018.06.048.
3. Ahmad, A., Saraswat, D., & El Gamal, A. (2023). A survey on using deep learning techniques for plant disease diagnosis and recommendations for development of appropriate tools. *Smart Agricultural Technology*, *3*, 100083. https://doi.org/10.1016/j.atech.2022.100083.
4. Bock, C. H., Poole, G. H., Parker, P. E., & Gottwald, T. R. (2010). Plant disease severity estimated visually, by digital photography and image analysis, and by hyperspectral imaging. *Critical Reviews in Plant Sciences*, *29*, 59–107. https://doi.org/10.1080/07352681003617285.
5. DadrasJavan, F., Samadzadegan, F., Seyed Pourazar, S. H., & Fazeli, H. (2019). UAV-based multispectral imagery for fast Citrus Greening detection. *Journal of Plant Diseases and Protection*, *126*, 307–318. https://doi.org/10.1007/s41348-019-00234-8.
6. Franke, J., & Menz, G. (2007). Multi-temporal wheat disease detection by multi-spectral remote sensing. *Precision Agriculture*, *8*, 161–172. https://doi.org/10.1007/s11119-007-9036-y.
7. Friedli, M., Kirchgessner, N., Grieder, C., Liebisch, F., Mannale, M., & Walter, A. (2016). Terrestrial 3D laser scanning to track the increase in canopy height of both monocot and dicot crop species under field conditions. *Plant Methods*, *12*, 9. https://doi.org/10.1186/s13007-016-0109-7.
8. Garcia, J., & Barbedo, A. (2013). Digital image processing techniques for detecting, quantifying and classifying plant diseases. *SpringerPlus*, *2*, 660. https://doi.org/10.1186/2193-1801-2-660.
9. Ghosal, S., Blystone, D., Singh, A. K., Ganapathysubramanian, B., Singh, A., & Sarkar, S. (2018). An explainable deep machine vision framework for plant stress phenotyping. *Proceedings of the National Academy of Sciences of the United States of America*, *115*, 4613–4618. https://doi.org/10.1073/pnas.1716999115.
10. Husin, N. A., Khairunniza-Bejo, S., Abdullah, A. F., Kassim, M. S. M., Ahmad, D., & Azmi, A. N. N (2020). Application of ground-based LiDAR for analysing oil palm canopy properties on the occurrence of basal stem rot (BSR) disease. *Scientific Reports*, *10*, 6464. https://doi.org/10.1038/s41598-020-62275-6.
11. Lazarević, B., Šatović, Z., Nimac, A., Vidak, M., Gunjača, J., Politeo, O., & Carović-Stanko, K. (2021). Application of phenotyping methods in detection of drought and salinity stress in basil (*Ocimum basilicum* L). *Frontiers in Plant Science*, *12*, 629441. https://doi.org/10.3389/fpls.2021.629441.
12. Manavalan, L. P., Cui, I., Ambrose, K. V., Panjwani, S., DeLong, S., Mleczko, M., & Spetsieris, K. (2021). Systematic approach to validate and implement digital phenotyping tool for soybean: A case study with PlantEye. *Plant Phenome Journal*, *4*, e20025. https://doi.org/10.1002/ppj2.20025.
13. Martin, F. N. (2000). Phylogenetic relationships among some Pythium species inferred from sequence analysis of the mitochondrially encoded cytochrome oxidase II gene. *Mycologia*, *92*, 711–727. https://doi.org/10.1080/00275514.2000.12061211.
14. Martinelli, F., Scalenghe, R., Davino, S., Panno, S., Scuderi, G., Ruisi, P., Villa, P., Stroppiana, D., Boschetti, M., Goulart, L. R., Davis, C. E., & Dandekar, A. M. (2015). Advanced methods of plant disease detection. A review. *Agronomy for Sustainable Development*, *35*, 1–25. https://doi.org/10.1007/s13593-014-0246-1.
15. Matthiesen, R. L., Ahmad, A. A., & Robertson, A. E. (2016). Temperature affects aggressiveness and fungicide sensitivity of four Pythium spp. That cause soybean and corn damping off in Iowa. *Plant Disease*, *100*, 583–591. https://doi.org/10.1094/PDIS-04-15-0487-RE.
16. McGehee, C. S., Raudales, R. E., Elmer, W. H., & McAvoy, R. J. (2019). Efficacy of biofungicides against root rot and damping-off of microgreens caused by Pythium spp. *Crop Protection*, *121*, 96–102. https://doi.org/10.1016/j.cropro.2018.12.007.
17. Minchinton, E., Petkowski, J., deBoer, D., Thomson, F., Trapnell, L., Tesoriero, L., Forsyth, L., Parker, J., Pung, H., & McKay, A. (2013). *Identification of IPM strategies for Pythium induced root rots in Apiacae vegetable crops*. Horticulture Australia Ltd.
18. Mulugeta Aneley, G., Haas, M., & Köhl, K. (2022). LIDAR-based phenotyping for drought response and drought tolerance in potato. *Potato Research*. https://doi.org/10.1007/s11540-022-09567-8.
19. Mutka, A. M., & Bart, R. S. (2015). Image-based phenotyping of plant disease symptoms. *Frontiers in Plant Science*, *5*, 734. https://doi.org/10.3389/fpls.2014.00734.
20. Nagasubramanian, K., Jones, S., Singh, A. K., Sarkar, S., Singh, A., & Ganapathysubramanian, B. (2019). Plant disease identification using explainable 3D deep learning on hyperspectral images. *Plant Methods*, *15*, 98. https://doi.org/10.1186/s13007-019-0479-8.
21. Nilsson, H. E. (1995). Remote sensing and image analysis in plant pathology. *Annual Review of Phytopathology*, *15*, 489–527. https://doi.org/10.1146/annurev.py.33.090195.002421.
22. Okubara, P. A., & Paulitz, T. C. (2005). Root defense responses to fungal pathogens: A molecular perspective. *Plant and Soil*, *274*, 215–226. https://doi.org/10.1007/1-4020-4099-7_11.
23. Paulitz, T. C. (1997). Biological control of root pathogens in soilless and hydroponic systems. *Hortscience*, *32*, 193–196. https://doi.org/10.21273/HORTSCI.32.2.193.
24. Pedregosa, F., Varoquaux, G., Gramfort, A., Michel, V., Thirion, B., Grisel, O., Blondel, M., Prettenhofer, P., Weiss, R., Dubourg, V., Vanderplas, J., Passos, A., Cournapeau, D., Brucher, M., Perrot, M., & Duchesnay, É. (2011). Scikit-learn: Machine learning in Python. *Journal of Machine Learning Research*, *12*, 2825–2830.
25. Qin, Z., & Zhang, M. (2005). Detection of rice sheath blight for in-season disease management using multispectral remote sensing. *International Journal of Applied Earth Observation and Geoinformation*, *7*, 115–128. https://doi.org/10.1016/j.jag.2005.03.004.

26. Rajan, P., Lada, R. R., & MacDonald, M. T. (2019). Advancement in indoor vertical farming for microgreen production. *American Journal of Plant Sciences*, *10*, 1397–1408. https://doi.org/10.4236/ajps.2019.108100.
27. Raji, S. N., Subhash, N., Ravi, V., Saravanan, R., Mohanan, C. N., MakeshKumar, T., & Nita, S. (2016). Detection and classification of mosaic virus disease in cassava plants by proximal sensing of photochemical reflectance index. *Journal of the Indian Society of Remote Sensing*, *44*, 875–883. https://doi.org/10.1007/s12524-016-0565-6.
28. Roberts, J. M., Bruce, T. J. A., Monaghan, J. M., Pope, T. W., Leather, S. R., & Beacham, A. M. (2020). Vertical farming systems bring new considerations for pest and disease management. *Annals of Applied Biology*, *176*, 226–232. https://doi.org/10.1111/aab.12587.
29. Salgadoe, A. S. A., Robson, A. J., Lamb, D. W., Dann, E. K., & Searle, C. (2018). Quantifying the severity of phytophthora root rot disease in avocado trees using image analysis. *Remote Sensing*, *10*, 226. https://doi.org/10.3390/rs10020226.
30. Singh, A., Jones, S., Ganapathysubramanian, B., Sarkar, S., Mueller, D., Sandhu, K., & Nagasubramanian, K. (2021). Challenges and opportunities in machine-augmented plant stress phenotyping. *Trends in Plant Science*, *26*, 53–69. https://doi.org/10.1016/j.tplants.2020.07.010.
31. Specht, K., Siebert, R., Hartmann, I., Freisinger, U. B., Sawicka, M., Werner, A., Thomaier, S., Henckel, D., Walk, H., & Dierich, A. (2014). Urban agriculture of the future: An overview of sustainability aspects of food production in and on buildings. *Agriculture and Human Values*, *31*, 33–51. https://doi.org/10.1007/s10460-013-9448-4.
32. Su, Y., Wu, F., Ao, Z., Jin, S., Qin, F., Liu, B., Pang, S., Liu, L., & Guo, Q. (2019). Evaluating maize phenotype dynamics under drought stress using terrestrial lidar. *Plant Methods*, *15*, 11. https://doi.org/10.1186/s13007-019-0396-x.
33. Suárez-Cáceres, G. P., Pérez-Urrestarazu, L., Avilés, M., Borrero, C., Lobillo Eguíbar, J. R., & Fernández-Cabanás, V. M. (2021). Susceptibility to water-borne plant diseases of hydroponic vs. *aquaponics systems Aquaculture*, *544*, 737093. https://doi.org/10.1016/j.aquaculture.2021.737093.
34. Sugiura, R., Tsuda, S., Tamiya, S., Itoh, A., Nishiwaki, K., Murakami, N., Shibuya, Y., Hirafuji, M., & Nuske, S. (2016). Field phenotyping system for the assessment of potato late blight resistance using RGB imagery from an unmanned aerial vehicle. *Biosystems Engineering*, *148*, 1–10. https://doi.org/10.1016/j.biosystemseng.2016.04.010.
35. Tian, Z., Ma, W., Yang, Q., & Duan, F. (2022). Application status and challenges of machine vision in plant factory—A review. *Information Processing in Agriculture*, *9*, 195–211. https://doi.org/10.1016/j.inpa.2021.06.003.
36. van Delden, S. H., SharathKumar, M., Butturini, M., Graamans, L. J. A., Heuvelink, E., Kacira, M., Kaiser, E., Klamer, R. S., Klerkx, L., Kootstra, G., Loeber, A., Schouten, R. E., Stanghellini, C., van Ieperen, W., Verdonk, J. C., Vialet-Chabrand, S., Woltering, E. J., van de Zedde, R., Zhang, Y., & Marcelis, L. F. M. (2021). Current status and future challenges in implementing and upscaling vertical farming systems. *Nature Food*, *2*, 944–956. https://doi.org/10.1038/s43016-021-00402-w.
37. Veys, C., Chatziavgerinos, F., AlSuwaidi, A., Hibbert, J., Hansen, M., Bernotas, G., Smith, M., Yin, H., Rolfe, S., & Grieve, B. (2019). Multispectral imaging for presymptomatic analysis of light leaf spot in oilseed rape. *Plant Methods*, *15*, 4. https://doi.org/10.1186/s13007-019-0389-9.
38. Waiphara, P., Bourgenot, C., Compton, L. J., & Prashar, A. (2022). Optical imaging resources for crop phenotyping and stress detection. In P. Duque, & D. Szakonyi (Eds.), *Methods in Molecular Biology* (2494 vol., pp. 255–265). Humana. https://doi.org/10.1007/978-1-0716-2297-1_18.
39. White, T. J., Bruns, T., Lee, S., & Taylor, J. W. (1990). Amplification and direct sequencing of fungal ribosomal RNA genes for phylogenetics. In M. A. Innis, D. H. Gelfand, J. J. Sninsky, & T. J. White (Eds.), *PCR Protocols: A Guide to Methods and Applications* (pp. 315–322). Academic Press, Inc.
40. Xiao, S., Chai, H., Shao, K., Shen, M., Wang, Q., Wang, R., Sui, Y., & Ma, Y. (2020). Image-based dynamic quantification of aboveground structure of sugar beet in field. *Remote Sensing*, *12*, 269. https://doi.org/10.3390/rs12020269.
41. Yamamoto, K., Togami, T., & Yamaguchi, N. (2017). Super-resolution of plant disease images for the acceleration of image-based phenotyping and vigor diagnosis in agriculture. *Sensors (Basel, Switzerland)*, *17*, 2557. https://doi.org/10.3390/s17112557.
42. Yang, C., Everitt, J. H., & Fernandez, C. J. (2010). Comparison of airborne multispectral and hyperspectral imagery for mapping cotton root rot. *Biosystems Engineering*, *107*, 131–139. https://doi.org/10.1016/j.biosystemseng.2010.07.011.
43. Yuan, H., Bennett, R. S., Wang, N., & Chamberlin, K. D. (2019). Development of a peanut canopy measurement system using a ground-based lidar sensor. *Frontiers in Plant Science*, *10*, 203. https://doi.org/10.3389/fpls.2019.00203.
44. Zhang, J., Huang, Y., Pu, R., Gonzalez-Moreno, P., Yuan, L., Wu, K., & Huang, W. (2019). Monitoring plant diseases and pests through remote sensing technology: A review. *Computers and Electronics in Agriculture*, *165*, 104943. https://doi.org/10.1016/j.compag.2019.104943.

Figures

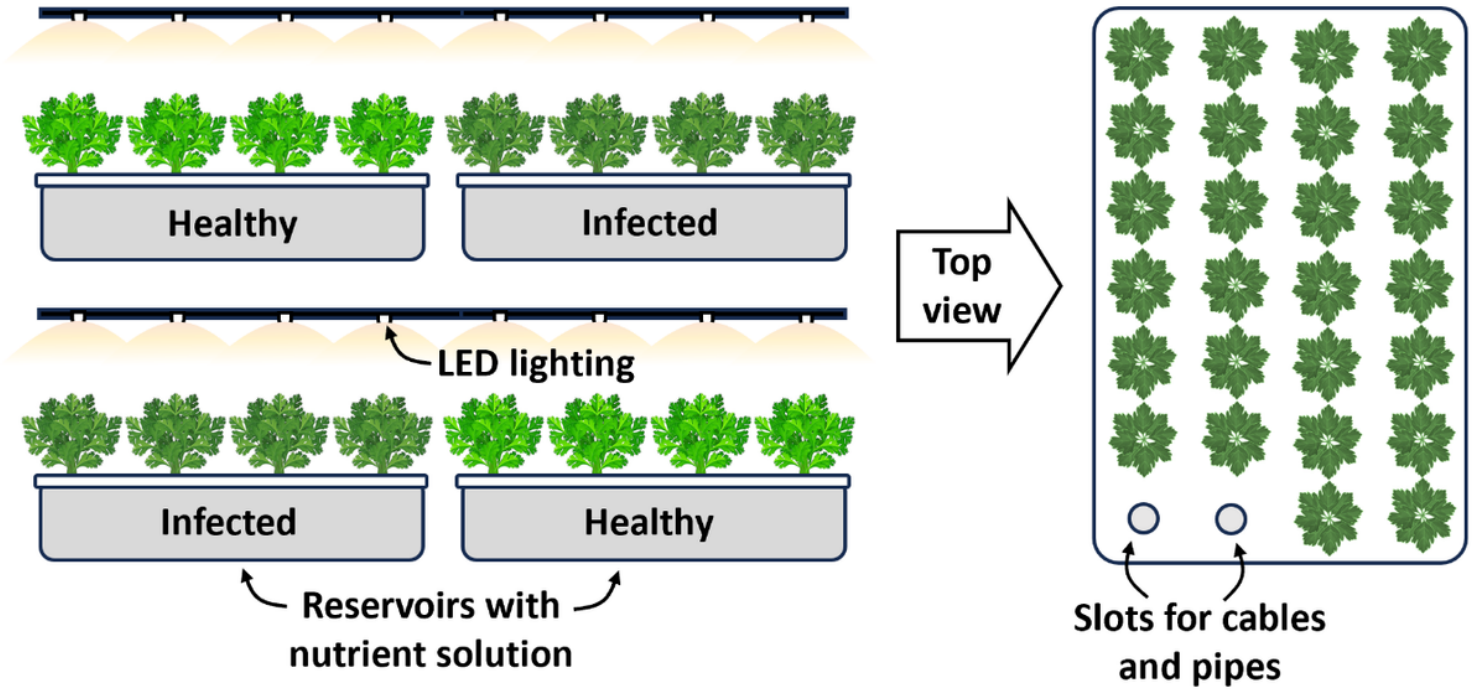

Figure 1

Schematic layout of the experimental vertical farming setup with “deep water culture” hydroponics. Empty slots in the tray were used for a cable connected to a submersible air pump (for root aeration) and a pipe with circulating water bath to maintain water temperature.

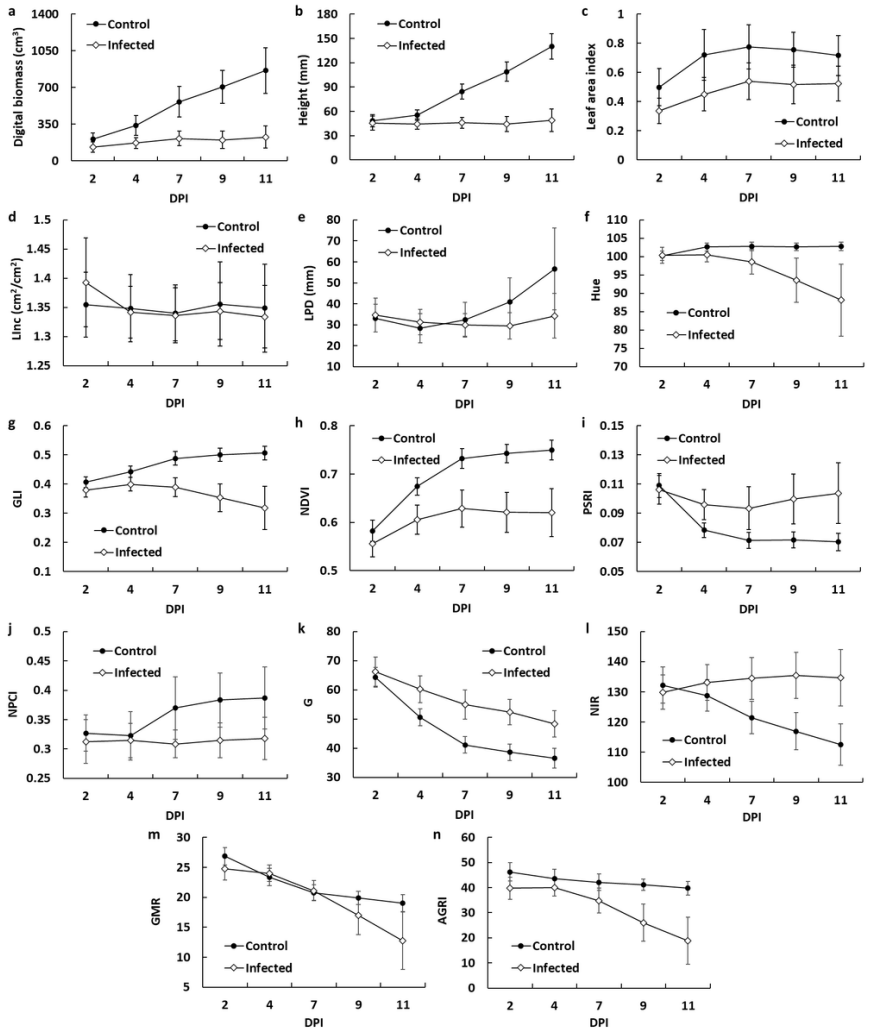

Figure 2

Digital biomass (a), plant height (b), leaf area index (c), leaf inclination (LInc; d), light penetration depth (LPD; e), Hue (f), Green Leaf Index (GLI; g), Normalised Difference Vegetation Index (NDVI; h), Plant Senescence Reflectance Index (PSRI; i), Normalised Pigment Chlorophyll ratio Index (NPCI; j), green reflectance (G; k), near-infrared reflectance (NIR; l), green-minus-red reflectance (GMR; m), and Augmented Green-Red Index (AGRI; n) of flat-leaf parsley infected with *P. irregulare* (main trial). Values have been expressed as mean ± SD (Control: n = 52; Infected: n = 52 for 2–7 DPI, n = 48 for 9 and 11 DPI).

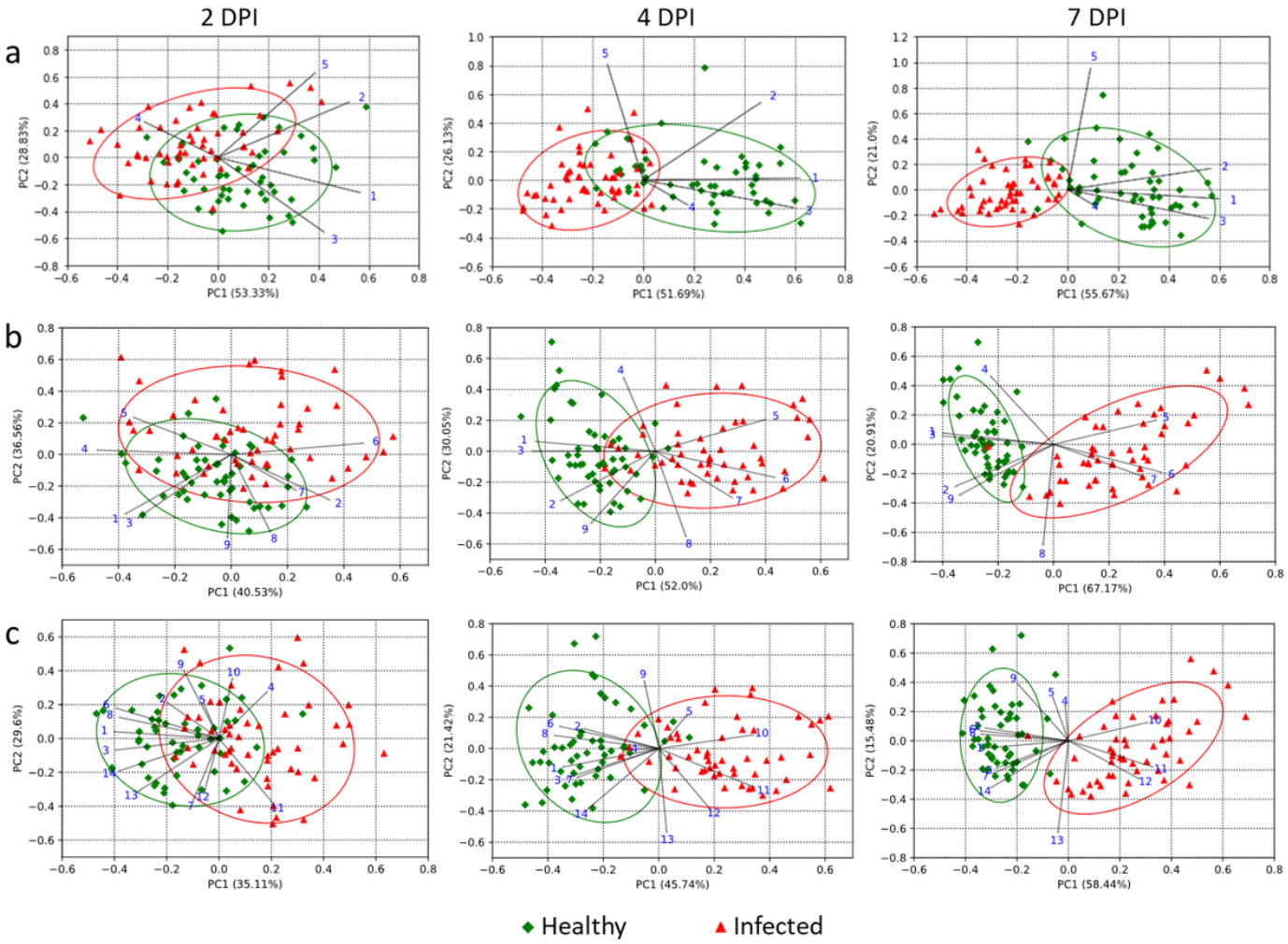

Figure 3

PCA of morphometric and spectral features for healthy (green, diamonds) and infected (red, triangles) plants at 2, 4, and 7 days post inoculation (DPI). Biplots represent the first two principal components (PCs) for the analyses with morphometric attributes (a; 5 features), spectral attributes (b; 9 features), and both datasets combined (c; 14 features). Values in parentheses indicate the percentage of variance explained by the corresponding PC. Ellipses represent the 95% confidence interval for each class, viz. healthy and infected (*n*= 52). Features are in the order: DB, Height, LAI, LInc, LPD (a; morphometric); GLI, Hue, NDVI, NPCI, PSRI, G, NIR, GMR, AGRI (b; spectral); morphometric followed by spectral in the same order (c). Plots for 9 and 11 DPI are presented in Online Resource 1: Fig. S3.

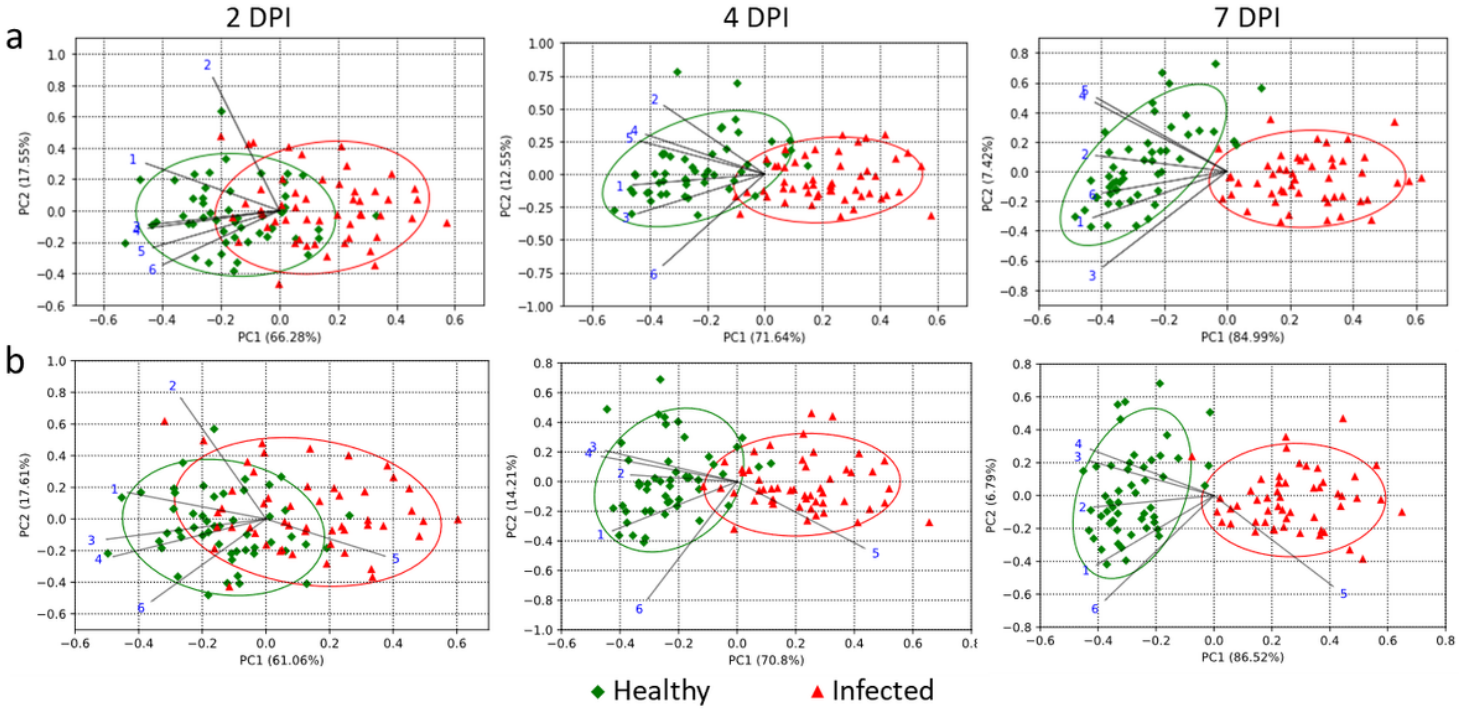

Figure 4

PCA of minimal datasets with specific morphometric and spectral attributes of healthy (green, diamonds) and infected (red, triangles) plants at 2, 4, and 7 days post inoculation (DPI). Biplots represent the first two principal components (PCs) for the analyses performed by combining three best morphometric and three best spectral features (a, MS_3-3), and top six features (b, MS_top6). Values in parentheses indicate the percentage of variance explained by the corresponding PC. Ellipses represent the 95% confidence interval for each class, viz. healthy and infected (n = 52). Features are in the order: DB, Height, LAI, GLI, NDVI, AGRI (a, MS_3-3); DB, Height, GLI, NDVI, G, AGRI (b, MS_top6). Plots for 9 and 11 DPI are presented in Online Resource 1: Fig. S4.

Supplementary Files

This is a list of supplementary files associated with this preprint. Click to download.

- ESM1.pdf